PERGAMON

Engineering Failure Analysis 6 (1999) 27–41

ENGINEERING FAILURE ANALYSIS

Determination of maximum allowable strain for polysilicon micro-devices

S.C. Bromley, L.L. Howell*, B.D. Jensen

Mechanical Engineering Department, Brigham Young University, Provo, UT 84602, U.S.A.

Received 30 July 1998; accepted 9 September 1998

Abstract

Polycrystalline silicon (polysilicon) is a material commonly used for micro-electro-mechanical systems (MEMS) for which reliable mechanical properties data is not available, especially for devices that have dimensions on the order of microns. This paper proposes a method for using test data that accounts for the uncertainties in mechanical properties and presents data from tests of polysilicon that may be used in the future design of polysilicon MEMS. The testing of 161 micro-devices to failure, results in a recommendation for design that the nominal strain be maintained below 0.0055.

Keywords: Brittle fracture; Electronic-device failures; Micro-mechanical systems; Strain analysis

1. Introduction

The design of devices that are reliable under load requires knowledge of the mechanical properties of the material. However, the design of micro-mechanical devices is hampered because the mechanical properties of many materials used in micro-electro-mechanical systems (MEMS) designs are not well understood at the micro level. Most MEMS are made using fabrication methods very similar to those used to make integrated circuits. The electrical properties of the materials used in these processes are very well understood, but the mechanical properties are not as well known. Polycrystalline silicon (polysilicon) is a common MEMS material for which reliable mechanical properties data is not available, especially for devices that have dimensions on the order of microns. Properties such as Young's modulus and strength are complicated by the fact that the device sizes often approach the grain size of the material. Because there are few grains in the particular member, there are not enough for the random orientation of multiple grains to cause the material to be isotropic. The testing of the mechanical properties of polycrystalline silicon then results in data with a large standard deviation.

* Corresponding author.

1350–6307/98/$ - see front matter
PII: S1350–6307(98)00028–4

This paper proposes a method for using strength test data that accounts for the uncertainties in mechanical properties and presents data from tests of polysilicon that may be used in the future design of polysilicon MEMS.

2. Background

Much more work has been done in recent years to better understand the mechanical properties of polysilicon. The properties of polysilicon have been tested a number of ways, including the deflection of beams using devices such as nanoindenters [1, 2] surface profilers [3] and torsion devices [4]. Sharpe et al. [5] tested 48 beams and found that the average Young's modulus was 169 ± 6.2 GPa. They also summarized the values for Young's modulus reported in various studies ranging from 123–175 GPa. Ballarini et al. [6] showed that the scatter of Young's modulus depended on the number of grains within a unit volume, the uncertainty increasing as the number of grains decreases; a model was also developed that predicts this variation [7]. Kahn et al. [8] and Ballarini et al. [9] investigated the fracture characteristics of thick polysilicon films.

3. Approach

To avoid failure, the maximum stress of a component should be kept below the stress at which failure occurs (the material strength). A common approach in design is to maintain the maximum stress, $\sigma_{\max}$, below the maximum allowable stress, $\sigma_{\text{allowable}}$, or

$$\sigma_{\max} \leqslant \sigma_{\text{allowable}} \tag{1}$$

where the maximum allowable stress is safely below the material strength.

If Young's modulus (E) is a constant (i.e. if the stress–strain curve is linear and $\sigma = E\varepsilon$) then an equivalent but less commonly used expression of eqn (1) may be stated as

$$\varepsilon_{\max} \leqslant \varepsilon_{\text{allowable}} \tag{2}$$

At the macro level, mechanical properties are often determined using tensile tests. Such tests are difficult at the micro level because of the sizes involved and because an accurate method of measuring the applied forces is not available. A second problem is that multiple tests would likely result in significantly different values of E, as shown by the findings of Mullen et al. [7]. The approach that follows was intended to take into account the inability to measure stress and the uncertainty in Young's modulus.

The method used involves loading the test specimens with a specified displacement rather than a force and ensuring that the displacements were large enough to be accurately measured optically. The strain may be calculated without knowing the Young's modulus of the material. This assumes that E is a constant, but the same strain results regardless of the magnitude of E. Each device was loaded until it fractured, the displacement at fracture was measured and the associated strain was calculated using a commercial finite element analysis program capable of non-linear analysis (ANSYS). This is possible because polysilicon is a brittle material and is assumed to fracture without going into a non-linear stress–strain regime. The strain data was used to try to identify

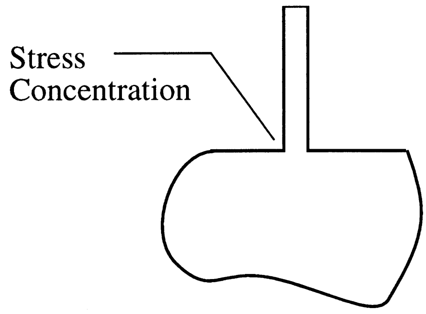

Fig. 1. A stress concentration typical in compliant MEMS devices.

trends and to determine an acceptable value for the allowable strain that can be used in future designs.

Stress concentrations are also common for surface micro-machined devices. A stress concentration (or stress raiser) is caused by an abrupt change in the geometry of a part under stress, such as shown in Fig. 1. The theoretical stress concentration may be determined from geometry alone, but it predicts a higher stress than is actually present. The actual stress concentration can be calculated from the theoretical stress concentration and the notch sensitivity of the material. Because the notch sensitivity is a mechanical property of the material, it is not known for polysilicon at the micro level. This problem is easily avoided by comparing the nominal strain (or stress) at a stress concentration to the nominal strain (or stress) at fracture. The nominal strain is the strain that would be calculated if there were no stress concentration.

Two studies were performed. The first study (Test 1) included the measurement of the strain at fracture for 61 polysilicon devices. These devices were originally designed to perform other functions. After these tasks were completed, the devices were fractured as part of this study. There was considerable scatter in the results. It was unclear how much of this was caused by the different geometries of the devices tested, or if it was from sources similar to those which cause uncertainty in the value of other material properties. The second study (Test 2) was performed to address the question of the scatter in the data and to determine if device geometry played a factor. At the macro level, geometry such as relative length, width, thickness and so on, would not be expected to have a significant effect on the nominal strain at fracture. However, because there was so much scatter in the data at the micro level for various geometries, the second study was designed not only to obtain strain data, but to investigate the possibility of geometry being a factor in the strain at fracture of micro-components.

3.1. Illustrative example

As an example of the approach used, consider the beam in Fig. 2. The actual compliant MEMS devices and micro beams tested were analyzed using non-linear analysis; however, for this illustrative example, a beam with small, linear deflections will be assumed to simplify the equations and to provide an explanation of the variables involved.

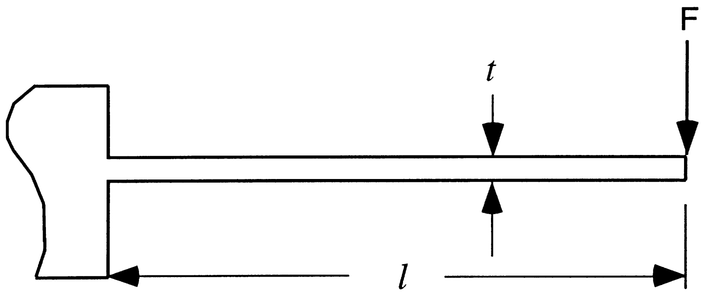

Fig. 2. A flexible beam with length l and thickness t.

If a force, F, is applied to the beam end, the nominal stress at the wall is

$$\sigma = \frac{Flt}{2I} \tag{3}$$

and the nominal strain is

$$\varepsilon = \frac{Flt}{2EI} \tag{4}$$

where I is the area moment of inertia and t and l are as shown in Fig. 2. The deflection of the beam end, δ, caused by the force is

$$\delta = \frac{Fl^3}{3EI} \tag{5}$$

The beam is deflected until failure occurs and the maximum deflection, $(\delta)_{\text{failure}}$, is recorded. The nominal strain at failure, $(\varepsilon)_{\text{failure}}$, is found by combining eqns (4) and (5) to eliminate the unknown force term and Young's modulus

$$(\varepsilon)_{\text{failure}} = \frac{3t}{2l^2}(\delta)_{\text{failure}} \tag{6}$$

Note that the nominal strain at failure may be calculated using only beam geometry and the deflection.

4. Test procedure

The theoretical approach described above was used to approximate the nominal strain at failure for flexible devices made of polysilicon using the MUMPs process [10]. Two separate studies were performed. In the first study (Test 1), several types of flexible devices were tested to failure, including flexible beams, compliant parallel-guiding mechanisms [11] and compliant straight-line mechanisms [12]. In Test 2, cantilevered beams were tested. The experimental designs for Tests 1 and 2 are described next, followed by a description of the test procedure used.

Table 1
Dimensions of the flexible beams (see Fig. 2)

Beam type	l (μm)	t (μm)
Beam-A	110	5
Beam-B	60	3
Beam-C	154	6
Beam-D	104	4
Beam-E	60	5

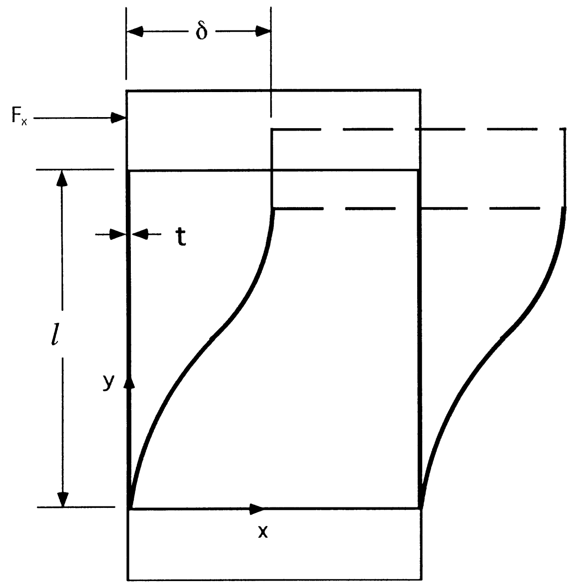

Fig. 3. A compliant parallel-guiding mechanism.

4.1. Test 1—flexible devices tested

Test 1 consisted of several types of devices. The flexible beams were constructed of 2 μm thick polysilicon, with lengths l and width t as shown in Fig. 2 and listed in Table 1. Twenty-eight configurations of the compliant parallel-guiding mechanism exist [11], two of which were used in this study. The first configuration has fixed connections at the ends of the flexible segments, as shown in Fig. 3. Three types of mechanisms of this configuration were used and the dimensions for each type are listed in Table 2. The second configuration of the compliant parallel-guiding mechanism includes flexible segments that are pinned to the ground, as illustrated in Fig. 4. Two types of mechanisms of this configuration were used and the dimensions for each type are listed in Table 3. Two types of compliant straight-line mechanisms were also used. These are illustrated in Fig. 5, with specific dimensions for each type listed in Table 4.

Table 2
Dimensions of the first configuration of parallel-guiding mechanisms (see Fig. 3)

Mechanism type	l (μm)	t (μm)
Parallel 1-A	100	4
Parallel 1-B	100	3
Parallel 1-C	150	3

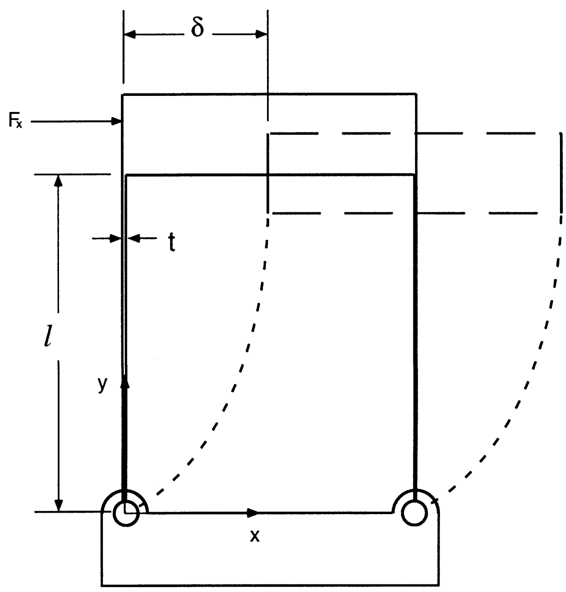

Fig. 4. A compliant parallel-guiding mechanism with two pin connections.

Table 3
Dimensions of the second configuration of parallel-guiding mechanisms (see Fig. 4)

Mechanism type	l (μm)	t (μm)
Parallel 2-A	150	3
Parallel 2-B	200	3

4.2. Test 2—beam design

In order to examine the nominal strain further, a full factorial experiment was conducted to determine if device geometry affects the nominal strain at failure. The full factorial design allowed the statistical examination of the singular and interactive effects of beam length, width, height and

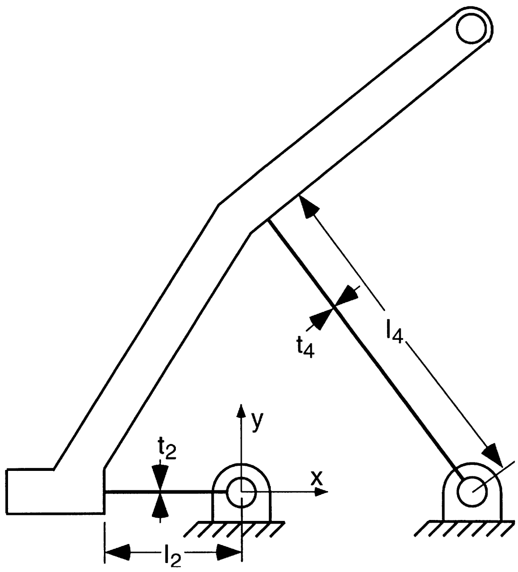

Fig. 5. A compliant straight-line mechanism.

Table 4
Dimensions of the compliant straight-line mechanisms (see Fig. 5)

Mechanism type	l_2 (μm)	t_2 (μm)	l_4 (μm)	t_4 (μm)
s1-A	47.1	3.0	117.6	3.0
s1-B	117.6	3.0	294.1	3.0

stress concentration on the nominal strain at beam failure. The beam design used for this study was modeled as a rigidly fixed cantilever. The micro beams were designed with lengths of 70, 135 and 200 microns, heights of 1.5, 2 and 3.5 microns, widths of 2 and 3 microns and either squared or chamfered junctions between the beam length and the anchor. All the possible combinations of these factors yielded 36 unique beam designs, all of which are listed in Table 5. A schematic of the general beam layout is shown in Fig. 6. The V-shaped notch directed the force applied by a probe tip into point loading. One half of the beams tested had a chamfer (Y) shown in Fig. 6, the other half did not (N). This chamfer was added to the experimental design to test how changing the stress concentration affects the failure strain.

The beams were fabricated in three randomized runs. A portion of the actual beams in Run 3 (R3) is shown in Fig. 7. Randomization and replication eliminate the influence of lurking variables on the test results. In the experiment, it was necessary to remove the effects of die release time, the beams' die placement and the beam testing. All three randomized runs, a total of 108 beams, were examined for this experiment.

Table 5
Summary of beam designs and strains for Runs 1–3 (all dimensions in μm)

Beam	Width	Chamfer	Length	Height	Strain Run 1	Strain Run 2	Strain Run 3
1	2	Y	70	1.5	0.0190	0.0159	0.0182
2	2	Y	70	2.0	0.0386	0.0170	0.0196
3	2	Y	70	3.5	0.0240	0.0222	0.0214
4	2	Y	135	1.5	0.0125	0.0154	0.0167
5	2	Y	135	2.0	0.0176	0.0266	0.0238
6	2	Y	135	3.5	0.0271	0.0248	0.0266
7	2	Y	200	1.5	0.0188	0.0101	0.0166
8	2	Y	200	2.0	*	0.0206	0.0240
9	2	N	200	3.5	0.0149	0.0210	*
10	2	N	70	1.5	0.0264	0.0177	0.0165
11	2	N	70	2.0	*	0.0194	0.0214
12	2	N	70	3.5	0.0243	0.0241	0.0266
13	2	N	135	1.5	0.0251	0.0207	0.0150
14	2	N	135	2.0	0.0236	0.0253	0.0243
15	2	N	135	3.5	0.0126	0.0105	0.0117
16	2	N	200	1.5	*	0.0228	0.0225
17	2	N	200	2.0	0.0211	0.0227	0.0160
18	2	N	200	3.5	0.0125	0.0148	0.0146
19	3	Y	70	1.5	0.0151	0.0111	0.0132
20	3	Y	70	2.0	0.0171	0.0141	0.0189
21	3	Y	70	3.5	0.0175	0.0164	0.0157
22	3	Y	135	1.5	*	0.0141	0.0141
23	3	Y	135	2.0	0.0234	0.0192	0.0190
24	3	Y	135	3.5	0.0154	0.0157	0.0163
25	3	Y	200	1.5	0.0123	0.0163	0.0189
26	3	Y	200	2.0	0.0232	0.0204	0.0215
27	3	Y	200	3.5	0.0182	0.0171	0.0170
28	3	N	70	1.5	*	0.0157	0.0148
29	3	N	70	2.0	0.0228	0.0164	0.0173
30	3	N	70	3.5	0.0146	0.0117	0.0187
31	3	N	135	1.5	0.0190	0.0177	0.0192
32	3	N	135	2.0	*	0.0250	0.0231
33	3	N	135	3.5	0.0199	0.0193	0.0192
34	3	N	200	1.5	0.0078	0.0159	0.0203
35	3	N	200	2.0	0.0206	0.0230	0.0211
36	3	N	200	3.5	*	0.0195	0.0183

* Beams that were broken during processing.

4.3. Testing

The devices were tested in the Integrated Microelectronics Laboratory at Brigham Young University. First, the die was mounted under an optical microscope. A micro-probe tip with

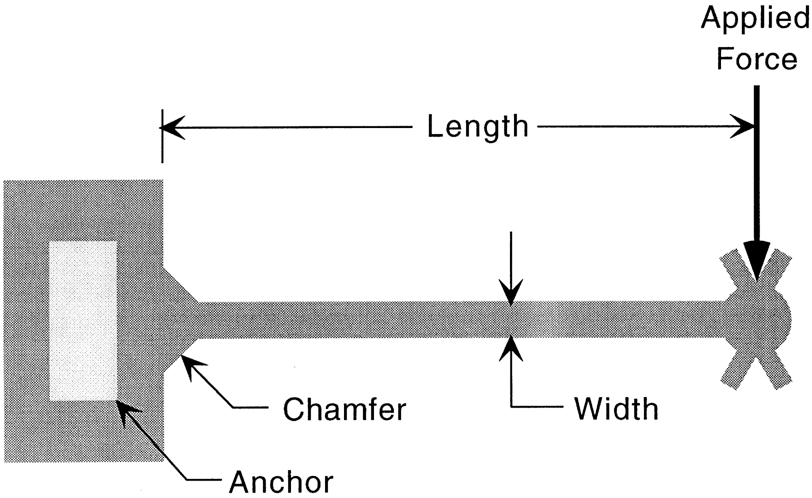

Fig. 6. Schematic of the beam design.

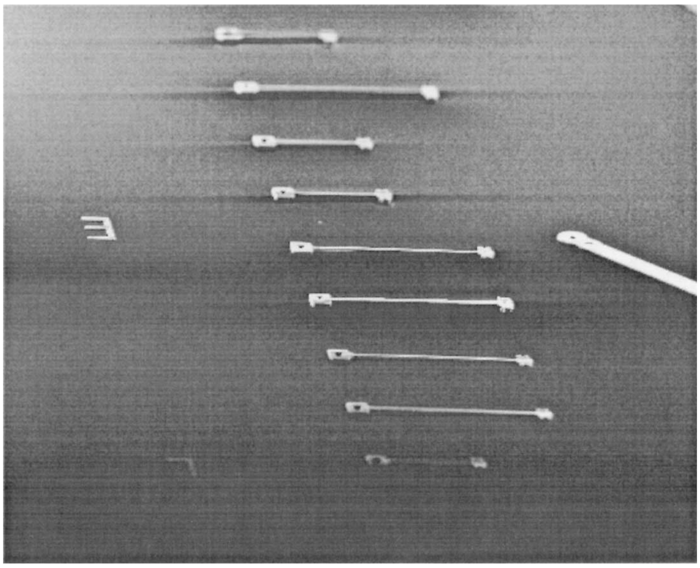

Fig. 7. SEM photograph of part of Run 3.

micrometer adjustments was used to deflect the devices to failure; the probe tip was directed onto the rigid coupler of the flexible device for Test 1; in Test 2, the probe tip was directed into the V-shaped notch. A VCR was used to record images sent from a CCD camera connected to the optical microscope. The recorded image was analyzed on a computer using a video board and motion analysis software. The deflection at failure was measured in pixels and converted to microns. A commercial finite element analysis program capable of non linear-deflection analysis was used to calculate the strain for the deflection at fracture. Because displacement loads are entered as the

Table 6
Nominal strain at fracture

Type	*N*	Mean	Maximum	Minimum	Standard deviation
Beam-A–E	14	0.019	0.025	0.012	0.0042
Parallel 1-A	6	0.016	0.019	0.015	0.0015
Parallel 1-B	14	0.019	0.026	0.014	0.0032
Parallel 1-C	6	0.012	0.013	0.010	0.0013
Parallel 2-A	4	0.0077	0.011	0.0051	0.0022
Parallel 2-B	5	0.0053	0.0064	0.0033	0.0012
s1-A	5	0.026	0.034	0.017	0.0078
s1-B	7	0.018	0.025	0.013	0.0049
Total	61	0.017	0.034	0.0033	0.0034

input load rather than forces, the strain is the same regardless of the value of Young's modulus used. This assumes that the stress–strain curve is linear and that the Young's modulus is the same for the entire structure.

The test devices were flexible and obtained deflections well into the nonlinear range. The large deflections were helpful in minimizing the measurement error since the deflections were much larger than the error associated with the imaging procedure used. However, the nonlinear deflections must be analyzed using numerical methods such as nonlinear finite element analysis since the linearized, small-deflection equations are not accurate for this situation.

5. Results

The following two sections report the results of Tests 1 and 2. A later section contains a summary of the data and discusses its usefulness in design.

5.1. Test 1

The number of each type of mechanism constructed (*N*) is listed in Table 6, as are the mean, maximum, minimum and standard deviations of the nominal strain at fracture for each mechanism type. The overall mean for all types tested was 0.017, with a standard deviation of 0.0034.

The nominal strains at failure for the second configuration of parallel mechanisms (Fig. 4) were well below the strains for the other mechanisms. Two major factors are believed to contribute to this condition. First, since two pin joints were used, the device fell to the substrate after release. The resulting stiction and friction forces between the mechanism and the substrate caused variations from mechanisms that do not experience those conditions. Second, the long flexible members may experience lateral torsional buckling, causing the members to fail sooner than would otherwise be the case. If the results for these mechanisms are not included, the mean nominal stress at failure would be 0.018. The minimum nominal strain would increase threefold to 0.010.

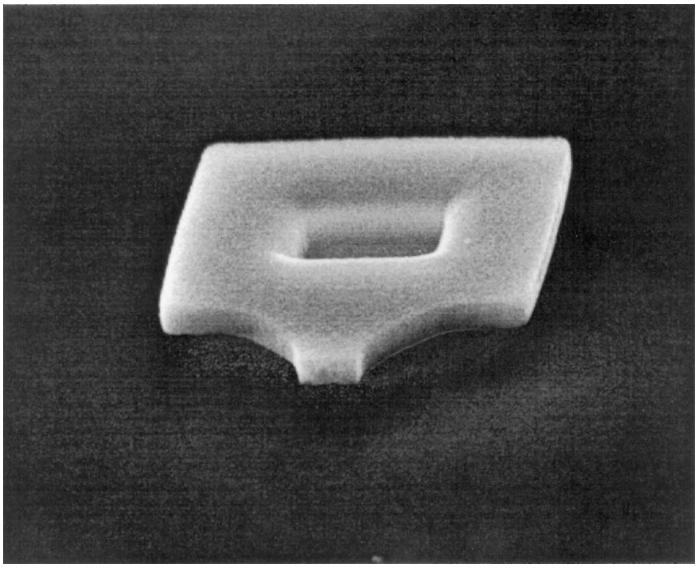

Fig. 8. SEM photo of typical micro beam fracture.

5.2. Test 2

Of the 108 beams, eight beams were broken during the die release. The remaining 100 beams were deflected until they fractured. A scanning electron microscope photograph of a typical fracture is shown in Fig. 8. A summary of the test data is in Table 5. The average strain for Test 2 over all samples is 0.0188 with a standard deviation of 0.0047. The median strain is 0.0188; 0.0386 is the maximum and 0.0078 is the minimum strain. The standard deviation is 25% of the average strain; this indicates significant scatter in the strain data. Figure 9 illustrates the scatter; it is a plot of the beam strains in order of magnitude. Notice how evenly the strain values are spread over the interval between 0.01 and 0.027. Instead of indicating a constant failure strain for polysilicon, the density of data points is fairly uniform over this range. A graph of beam type vs strain is presented in Fig. 10. Note the lack of trends in the data. The beams with close correlation, meaning all beam data points exhibit nearly the same strain, do not have any specific characteristics in common. After a statistical analysis and an examination of the data trends, it was determined that the variations in beam geometry did not affect the nominal strain. This is consistent with what occurs at the macro level.

6. Discussion of error

Seeing the significant scatter in the strain data, one must address whether the scatter is due to micro phenomena or to the error inherent in the testing techniques and analysis. The errors introduced in fabrication, loading and data analysis were examined.

Because the beam load was applied by a manually operated probe tip, the loading was not always perfectly directed. In Test 1, any force applied at a distance from the center of the rigid

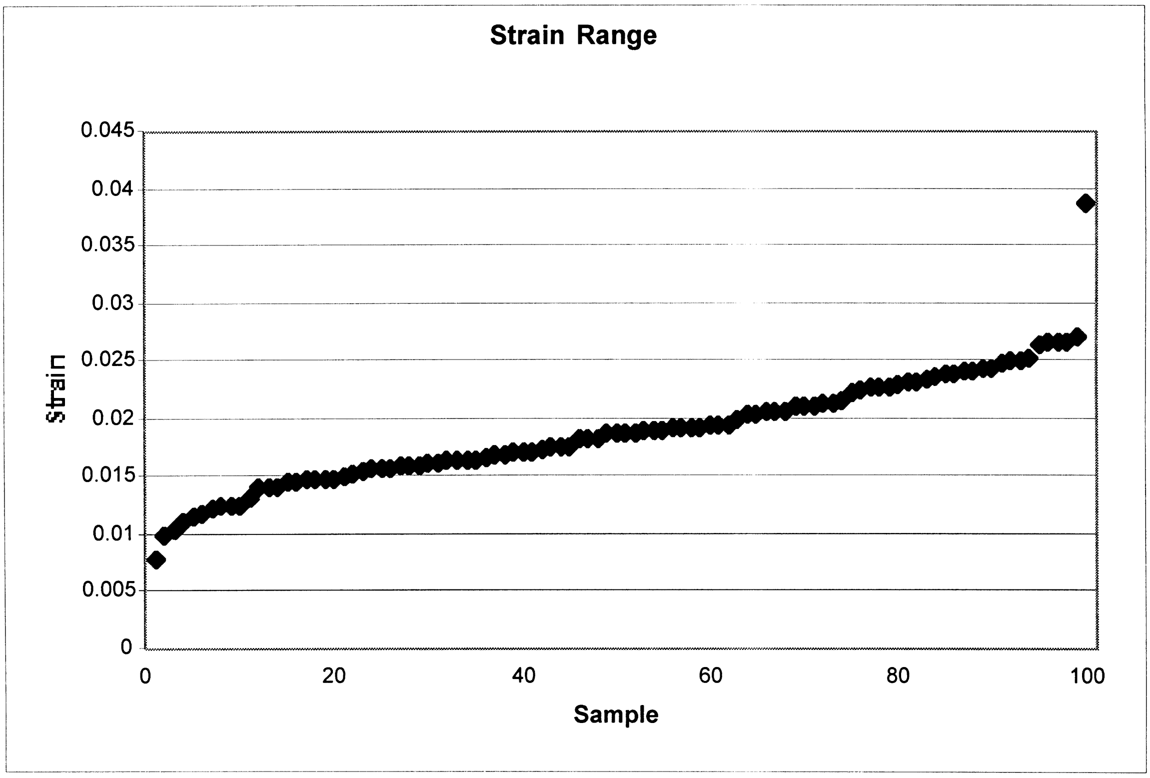

Fig. 9. Plot of beam strains in order of strain magnitude.

coupler link resulted in an additional moment on the head of the beam. This problem led to the V-shaped notch design implemented in Test 2. However, because the length of the rigid link side, the notch length and the average force applied to the beam are all extremely small, this source of error is also insignificant.

Finally, the error resulting from measuring the movement of the beam in pixels and manually picking the beam end in the motion analysis system were analyzed. For the pixelized measurement the end point of the beam was assumed to be in the direct center of the pixel in which it fell. In manually picking the end point of the beam, the researcher's placement was not always exact. The effect of these possible errors was quantified by recalculating the strain in eight positions at the extremes of the possible beam end positions. For the worst case the difference in strains was only 8.65%. This is still far below the scatter shown by the standard deviation; the possible errors cannot account for scatter in the strain data.

7. Implications for design

Combining the results of the two tests, the average nominal strain is 0.0181 and the average standard deviation is 0.0042 as shown in Table 7. These results may be used in a number of

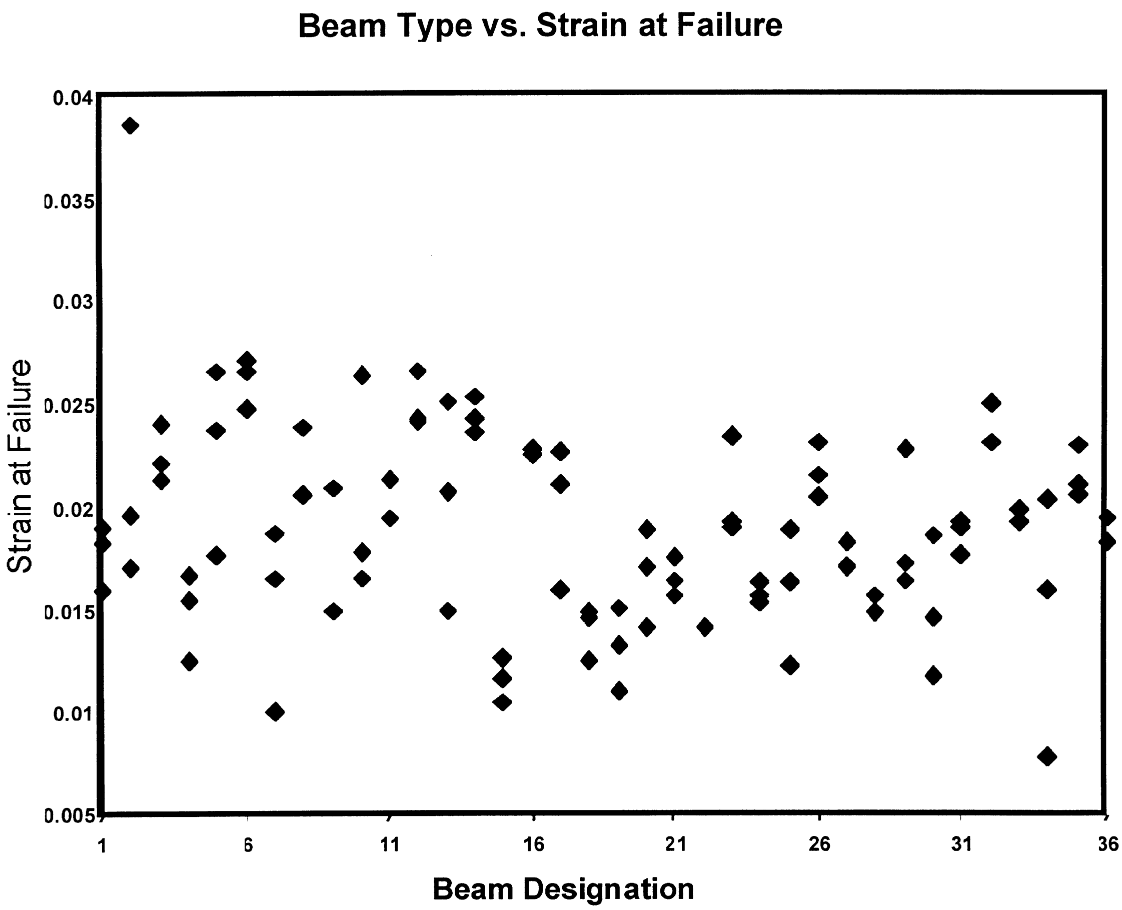

Fig. 10. A plot of the beam type (Table 5) vs the measured strain in Runs 1–3.

Table 7
Comparison of strain statistics

	Test 1	Test 2	Total
Data points	61	100	161
Average	0.0170	0.0188	0.0181
Minimum	0.0033	0.0078	0.0033
Maximum	0.0340	0.0386	0.0386
Standard deviation	0.0034	0.0047	0.0042

different ways in the design of MEMS devices. The mean nominal strain at failure may be used in design in a manner similar to how the fracture strength would be used.

One approach is to ensure that the nominal strain is less than the mean nominal strain at fracture minus three standard deviations, or:

$$\varepsilon_{\mathrm{max}} \leqslant (\varepsilon)_{\mathrm{failure}} - 3^{*}(\text{standard deviation}) \tag{7}$$

For the results presented in this paper

$$\varepsilon \leqslant 0.0055 \tag{8}$$

or

$$\varepsilon_{\mathrm{allowable}} = 0.0055 \tag{9}$$

Sometimes it is more convenient to use a value of strength in design. For a Young's modulus of $E = 169$ GPa, the nominal allowable stress is

$$\sigma_{\mathrm{allowable}} = 930 \text{ MPa} \tag{10}$$

This is comparable to the strength of many high strength steels at the macro level.

8. Conclusion

The nominal strain at failure for polysilicon has been investigated. The approach used includes deflecting a component to failure, measuring the deflection and calculating the corresponding nominal strain. The mean nominal strain for the 161 polysilicon devices tested was 0.0181, with a standard deviation of 0.0042.

The scatter in the data is most likely due to the small number of grains in a given test specimen. The uncertainty in material properties increases as the number of grains decreases because there are not enough grains in the specimen for grain randomization to cause consistent properties. Another possible source of variability in the data is the distribution of micro-defects in the grains in the beams. Because the beams are so narrow, with small volume, they may not have a constant distribution of defects from beam to beam. A defect in one beam may cause failure sooner, while a lack of significant defects in another may cause failure later.

In design, it is recommended that the maximum nominal strain of a device be kept below the allowable strain that can be taken to be the mean strain minus three standard deviations, or 0.0055.

Acknowledgements

The authors express their appreciation to Linton Salmon and the staff of the Integrated Microelectronics Laboratory for their assistance in this work. The help of Daniel Gunyan, Dani Johnson, Brian Christensen and Darrin Stokes in obtaining test data is gratefully acknowledged, as is the help of Nathan Masters in obtaining the SEM photographs. This work was supported by the National Science Foundation (NSF) under Grant No. ECS-9528238, an NSF CAREER Award under Grant No. DMI-9624574, an NSF Graduate Fellowship and the Office of Research and Creative Activities at Brigham Young University.

References

[1] Weihs TP, Hong S, Bravman JC, Nix WD. Mechanical deflection of cantilever micro beams: a new technique for testing the mechanical properties of thin films. Journal of Materials Research 1989;3(5):931–42.
[2] Vinci RP, Bravmen JC. Mechanical testing of thin films. IEEE Microelectro-mechanical Systems, 1991, pp. 943–8.
[3] Tai Y-C, Muller RS. Measurement of Young's modulus on micro-fabricated structures using a surface profiler. 1990 IEEE Micro-electro-mechanical Systems, 1990, pp. 147–52.
[4] Saif MTA, MacDonald NC. Micro-mechanical single crystal silicon fracture studies—torsion and bending. Proceedings of the IEEE Ninth Annual International Workshop on Micro-electro-mechanical Systems. San Diego, CA, 1996, pp. 105–9.
[5] Sharpe WN, Yuan B, Vaidyanathan R. Measurements of Young's modulus, Poisson's ratio and tensile strength of polysilicon. IEEE Micro-electro-mechanical Systems, 1997, pp. 424–9.
[6] Ballarini R, Mullen RL, Kahn H, Stemmer S, Heuer AH. Fracture energy and elastic constants of polycrystalline silicon thin films for micro-electro-mechanical systems (MEMS). Proceedings of the 1997 NSF Design and Manufacturing Grantees Conference. Seattle, WA, 1997, pp. 563–4.
[7] Mullen RL, Ballarini R, Yin Y, Heuer AH. Monte Carlo simulation of effective elastic constants of polycrystalline thin films. Acta mater. 1997;45(6):2247–55.
[8] Kahn H, Stemmer S, Nandakumar K, Heuer AH, Mullen RL, Ballarini R, Huff MA. Mechanical properties of thick, surface micro-machined polysilicon films. Proceedings of the IEEE Ninth Annual International Workshop on Micro-electro-mechanical Systems. San Diego, CA, 1996, pp. 343–8.
[9] Ballarini R, Mullen R, Yin Y. The fracture toughness of polysilicon micro-devices: a first report. Journal of Materials Research 1997;12(4):915–22.
[10] Mehregany M, Dewa AS. Introduction to micro-electro-mechanical Systems and the Multiuser MEMS Processes. Cleveland, OH: Case Western Reserve University, 1993.
[11] Derderian JM, Howell LL, Murphy MD, Lyon SM, Pack SD. Compliant parallel-guiding mechanisms. Proceedings of the 1996 ASME Mechanisms Conference. Paper 96-DETC/MECH-1208, 1996.
[12] Jensen BD, Howell LL, Gunyan DB, Salmon LG. The design and analysis of compliant MEMS using the pseudo-rigid-body model. Micro-electro-mechanical Systems (MEMS), at the 1997 ASME International Mechanical Engineering Congress and Exposition, DSC-Vol. 62, pp. 119–26.